Kache and Hendrix *BMC Methods* (2025) 2:17
https://doi.org/10.1186/s44330-025-00039-2

BMC Methods

METHODOLOGY Open Access

H^{2}MM-guided removal of dye blinking effects from single-molecule FRET burst data

Tom Kache[1] and Jelle Hendrix[1*]

Abstract

Background Confocal burst single-molecule FRET (smFRET) is a valuable technique for studying biomolecular dynamics over various timescales. Photon-by-photon recording and analysis approaches, such as multiparameter Hidden Markov analysis (mpH^{2}MM), exploit the full time resolution of the data and allow disentangling FRET-related signal changes from fluctuations caused by dye-related phenomena, such as blinking. However, the influence of blinking dynamics on quantitative mpH^{2}MM analysis has not been explored in detail.

Methods Using simulated smFRET data, we characterized the impact of blinking dynamics on quantitative mpH^{2}MM analysis. We developed an mpH^{2}MM-guided approach to remove the subset of bursts affected by blinking. We systematically validated our approach with simulations and applied it to experimental confocal burst smFRET data of DNA hairpins.

Results We demonstrated that standard-processed smFRET data from a dynamic DNA hairpin contain dye-blinking states. Since the true parameters in experimental data are unknown, we used simulations with different severities of blinking to characterize the impact of dye-blinking dynamics on mpH^{2}MM analysis. We showed that blinking causes mpH^{2}MM to systematically underestimate FRET state exchange rates and shift the $E-S$ histogram. We applied our proposed mpH^{2}MM-cleaning approach to simulated data with various degrees of blinking dynamics. Removing blinking-affected bursts corrected the blinking-induced bias in the $E-S$ plot and mitigated the blinking bias of mpH^{2}MM analysis. Finally, we demonstrated the effect of the filtering approach on experimental smFRET data of a dynamic DNA hairpin and observed similar effects to those in simulated data.

Discussion We propose a method to minimize the impact of dye blinking on dynamic smFRET analysis by using the ability of mpH^{2}MM to identify short-lived dye blinking states. Removing blinking-affected bursts improved the accuracy of dynamic smFRET analysis and enabled accurate recovery of state exchange rates by subsequent mpH^{2}MM analysis, though at the cost of losing affected bursts. Our findings highlight the importance of considering dye blinking effects in qualitative and quantitative smFRET analysis and the critical need to combine alternating-excitation smFRET with photon-by-photon analysis.

Keywords Single-molecule FRET, Photon-by-photon analysis, Fluorescent dye blinking, Biomolecular dynamics

*Correspondence:
Jelle Hendrix
jelle.hendrix@uhasselt.be
[1]Dynamic Bioimaging Lab, Hasselt University, Diepenbeek 3590, Belgium

Introduction

Dynamic structural rearrangements of biomolecules are essential to their function [1–5] and occur in many, if not all, classes of biomolecules, such as enzymes [6–9], membrane proteins [10, 11], or nucleic acids [12–16]. As structural dynamics are not easily synchronized over a bulk of molecules but rather appear as quasi-random, jump-like processes at the level of individual molecules, ensemble averaging experimental techniques such as X-ray crystallography, Small-angle X-ray scattering, or cuvette-based fluorescence spectroscopy cannot resolve such phenomena. Single-molecule techniques, such as single-molecule Förster resonance energy transfer (smFRET), overcome these limitations by directly measuring individual molecules [1, 17–19]. FRET relies on non-radiative energy transfer between a donor and acceptor dye, with changes in the transfer efficiency reflecting changes in inter-dye distance [3, 19, 20] is a useful phenomenon for detecting structural changes in biomolecules by monitoring nanometer-scale distances in real-time [1, 17]. The donor and acceptor dyes used for FRET experiments are typically site-specifically conjugated to informative sites on the molecule of interest [21–23]. Single-molecule detection in smFRET is commonly achieved by tethering the molecule to a surface for extended observation times or by analyzing the signal of molecules as they freely diffuse through the detection volume on a confocal microscope [1, 2].

In diffusion-based confocal smFRET (from hereon referred to as "smFRET"), picomolar concentrated fluorescently labeled molecules appear one at a time as sudden spikes in fluorescence intensity, known as bursts. They result from the Brownian diffusion of fluorescently labeled molecules through the confocal observation volume of the smFRET instrument [24, 25]. For typically-sized biomolecules, bursts last a few milliseconds and are algorithmically extracted to build burst-wise FRET histograms, where the FRET-detectable states of individually observed molecules appear as distinct populations. Various analysis methods have been developed to extract kinetic and structural information from burst smFRET data, for example, approaches that assess the variance of the FRET traces within bursts (e.g., burst variance analysis, BVA [26]), analysis of the histogram shape given a kinetic model (e.g., photon distribution analysis PDA [27, 28]), or time-correlation of the fluorescence signal (e.g., filtered fluorescence correlation spectroscopy, fFCS [29, 30]). However, in many, if not all of methods, the donor and acceptor dyes are, in most cases, assumed to be perfect fluorophores.

Blinking is a common phenomenon exhibited by fluorescent dyes and refers to the observation that dyes temporarily stop to fluoresce entirely or alter their emission properties. Blinking typically occurs on timescales of micro- to milliseconds and its rate depends on the type of fluorophore, its local environment, and excitation intensity [2, 31–33]. In smFRET experiments, blinking of the acceptor dye in particular, may be misinterpreted as a structural transition because a loss in acceptor intensity appears as a loss of FRET [34, 35]. Alternating excitation schemes were introduced to monitor the acceptor dye [25, 36, 37]. However, if blinking fluctuations occur on a timescale close to or faster than the duration of a burst, they are still contained in the burst-wise data. Several ways have been proposed to mitigate the impact of dye blinking. This includes chemical stabilization of the dyes by using, for example, an oxygen scavenging system or different classes of dyes [31, 33, 34]. Also, computational filters, such as ALEX-2CDE, were developed to differentiate bursts containing fluctuations in their acceptor excitation signals [38].

With photon-by-photon analysis quickly gaining popularity in the field, a detailed investigation of the influence of dye blinking on analysis accuracy becomes critical. In the original publication on H^2MM by Pirchi and coworkers, for example, the authors demonstrated that acceptor blinking indeed influences the obtained exchange rate under experimental conditions that increased the acceptor blinking probability [39]. Similarly, Harris and coworkers showed that with alternating excitation smFRET data, dye blinking states can be captured and differentiated from FRET-informative states [11, 40–42]. Monitoring and dealing with dye blinking, in principle, requires preserving single photon resolution up to the point where kinetic modeling is carried out. However, in the common smFRET analysis methods such as bursts histogramming, BVA, binwise PDA and fFCS, this resolution is lost by averaging the photons of part of or an entire burst. Recently, photon-by-photon analysis methods were put forward to preserve the time resolution of the data, ultimately only limiting the smFRET time resolution by the measurement instrumentation [43, 44]. Specific to smFRET, in such methods the momentary state of biomolecules is inferred as state-associated patterns of photons across the available detectors of the instrument. Ultimately, photon-by-photon methods aim to obtain a model that explains the observed photons given certain biomolecular states and dynamics. The Hidden Markov Model framework, for example, has been adapted and applied to single photon smFRET data by Pirchi and coworkers [8, 39]. The approach was termed H^2MM and later extended by Harris and coworkers to an arbitrary number of photon streams, such as alternating excitation, polarization-, and lifetime-resolved data, and termed multiparameter H^2MM (mpH^2MM) [40, 45]. With the latter methods, the mean state-wise parameters, state connectivity, and exchange rates are determined by obtaining the average time spent in a particular state and

the corresponding state transition pathways. The most likely number of states can be determined using the ICL and BIC criteria within the framework of Hidden Markov models, where the optimal model assumes the lowest value [40].

In this study, we systematically evaluated the impact of dye blinking on mpH^{2}MM. Using simulated alternating excitation smFRET data, we established that blinking dynamics biases the exchange rate between FRET states as resolved by mpH^{2}MM. Next, we demonstrated a simple yet effective mpH^{2}MM-based workflow for identifying and excluding bursts affected by dye blinking from alternating excitation smFRET data. Finally, we applied our approach to simulated and experimental data of a dynamic DNA hairpin. We showed that removing blinking contaminated bursts restored mpH^{2}MM's ability to accurately recover exchange rates, establishing mpH^{2}MM as an effective tool for smFRET analysis devoid of blinking-related artifacts.

Methods

Labeled dynamic DNA hairpin

The design for the dynamic DNA hairpin was adapted from Tsukanov et al. [46]. The DNA hairpin was composed of two sequences, `5′-XGG ATT (AAA)`$_{11}$ `TCC ATT TTC TTC ACA AAC CAG TCC AAA CTA TCA CAA ACT TA-3′` and `5′-(Biotin)-TTT TTA AGT TTG TGA TAG TTT GGA CTG GTT YGT GAA GAA-3′` with X and Y as ATTO 643-dT and Alexa-Fluor 488-dT, respectively (Ella Biotech, Germany). The labeled oligonucleotides ($1\ \mu M$ each) were annealed in TE buffer (10 mM Tris-HCl pH 8, 1 mM EDTA) containing $50\ mM$ NaCl by heating the solution to $95°C$ for 5 minutes and then cooling to room temperature. The annealed DNA hairpins were stored at $-20°C$.

Experimental smFRET measurements

Burst smFRET data was obtained with a home-built multiparameter, single-photon detection confocal microscope operated in pulsed-interleaved excitation mode10 with laser diodes at 483 and 635 nm (LDH-P-C-470, Picoquant and LDH-P-C-635B, Picoquant) pulsing at 26.67 MHz (Picoquant PDL 828 "Sepia II" laser driver). The laser powers were adjusted to 100 and 50 µW for the 483 and 633 nm lasers, respectively (measured between the excitation polychroic mirror and the objective lens, about 80% of this power reached the sample). The 635-nm laser was delayed by 18 ns with respect to the 483-nm laser. Sample fluorescence was collected with a UPLSAPO-60XW objective lens (Olympus), passed through a 75-µm pinhole, and split by spectrum using a dichroic mirror. Each spectral range was further split by polarization. The fluorescence signal was detected using four avalanche photodiodes (PD-100-CTE, MPD and SPCM-AQR, Perkin-Elmer for the 483 and 635-nm emissions, respectively) and recorded with a time-correlated single-photon counting device (Becker&Hickl SPC-630). System alignment was carried out by measuring the molecular brightnesses of aqueous solutions of ATTO 488-COOH and ATTO 655-COOH. Brightnesses of $> 90\ kHz$ for ATTO 488-COOH and $> 70\ kHz$ for ATTO 655-COOH were accepted. The DNA hairpin samples were diluted in STE buffer (10 mM Tris-HCl pH 8, 1 mM EDTA, 500 mM NaCl) to about 50 pM. The objective lens was focused about 100 µm into the measurement solution. smFRET data were recorded at room temperature ($23\ °C$) for 30 to 60 minutes.

smFRET data processing and burst search

Experimental, recorded in the Becker&Hickl.spc format, and simulated smFRET data were converted to the photon-HDF5 format using the phconvert [47] module.

First, the pulsed-interleaved excitation photon streams were defined using the corresponding nanotime ranges to yield $D_{ex}D_{em}$, $D_{ex}A_{em}$, and $A_{ex}A_{em}$ (D and A referring to the donor and acceptor spectral channels, respectively; the subscripts *ex* and *em* refer to the excitation laser and the fluorescence emission; for example, $D_{ex}A_{em}$ is the detected acceptor signal upon excitation of the donor). Further processing and burst search was performed by loading an experimental or simulated dataset into the FRETBursts [48, 49] module. First, the background count rate was estimated with a 30-second time window. An all-photon burst search was conducted with a sliding window containing 10 consecutive photons ($m = 10$) and an acceptance threshold of at least six times the background count rate. The resulting list of bursts now contains all events regardless of whether a burst only contained donor or acceptor signal. Next, the list of bursts was further filtered to exclude very short events as well as events that only contain donor or acceptor signal. this was achieved by requiring at least 60 photons in the $D_{ex}D_{em}$ and $D_{ex}A_{em}$ photon streams (using the `.size` selection method of FRETBursts with the `add_naa` flag set to `False`). This requirement ensured that a certain amount of FRET-relevant information is present in the retained datasets. To further remove bursts that predominantly contained donor-only contributions, for example, due to incomplete labeling or bleaching, a minimum of 40 photons was required in the $A_{ex}A_{em}$ photon stream (by using the `.naa` selection method of FRETBursts). The abscence of donor- and acceptor-only bursts was confirmed visually by checking that no bursts landed on the ES plot in the region of S 1 and E 0 (for donor-only bursts) and S 0 and E 0.5 (for acceptor-only bursts). No corrections were applied to the presented data. ALEX-2CDE filtering was done by running the data additionally through a filter function (the corresponding function

was taken from https://github.com/OpenSMFS/FRETBursts/blob/master/notebooks/Example%20-%202CDE%20Method.ipynb). If not stated otherwise, an ALEX-2CDE time constant of 150 μs was chosen. Moderate filtering was done by accepting bursts with an ALEX-2CDE filter value > 80, more strict filtering was achieved by requiring a valued > 100. Dual-color burst search (DCBS) [50] was performed with built-in functions of the FRETbursts module (following the FRETBursts tutorial, see) with a 10 photons time window (m) and an acceptance threshold of at least 7−times the background count rate (F). A total number of at least 80 photons in the $D_{ex}D_{em}$ and $D_{ex}A_{em}$ photon streams was required.

mpH^{2}MM analysis and mpH^{2}MM-cleaning of blinking dynamics

The list of burst events obtained from FRETbursts was passed to the burstH2MM module [40, 51] to perform mpH^{2}MM analysis. The optimal number of states from an mpH^{2}MM run was assessed by plotting the values of the ICL and BIC' parameters, where with a given number of states, a minimum value or a value < 0.005, respectively, was taken as evidence for the correctness of the corresponding number of states. The transition matrix of the best-fitting model from mpH^{2}MM analysis was printed to assess and document the values for E and S of the identified states and the obtained transition rate between states. The results from mpH^{2}MM analysis were visualized as state-wise plots using the burstH2MM module, which display the average E and S parameters of individual states, i.e. the time a molecule was identified by mpH^{2}MM to be in a particular state, rather than burst-averaged parameters. The transition rates between states are visualized as arrows between the average E and S values for each state which are plotted as red dots.

To remove bursts that contain blinking states (i.e. to carry out mpH^{2}MM cleaning), a mpH^{2}MM was chosen which exhibited a clear difference in stoichiometry between the supposed donor-only (with $S \approx 1$), acceptor-only ($S \approx 0$), and FRET-active states ($S \approx 0.5$). After model fitting with the burstH2MM module, each burst gets assigned a trajectory of states which, given the optimal number of states was correctly chosen, described the transition of the burst through different states. Each state is identified by a number. A custom-written function is used to search through the list of numbers in the mpH^{2}MM model and returns the indices of those bursts that were identified in the desired states. This is done in a way that allows specifying whether bursts should be selected that were only found in one particular states or in several over the course of their burst duration. In order to remove blinking events, typically, the four-state model is used and the states are supplied to the custom written function that allow selecting bursts that were identified as having visited the low FRET, high FRET, as well as both low and high FRET in their burst duration. This effectively removes those bursts which were at any point found in a non-FRET-active state (judged by the stoichiometry of the states). The resulting selection mask is used to discard bursts that contained blinking dynamics. A new FRETBursts object with the remaining bursts was created for subsequent visualization and analysis.

Simulation procedure of smFRET data with FRET and blinking dynamics

The simulation approach was adapted and expanded from existing Jupyter notebooks published by Harris et al. (2022, see DOI: 10.5281/zenodo.4671392) [40, 51]. The approach is first described, and then the exact parameters used to obtain the simulation files presented in this paper are given (see section Parameters for the Presented Simulations). The corresponding Jupyter notebooks are available in the supplementary materials.

The PyBromo [52] module was used to generate a particle diffusion trajectory in a simulation box with periodic boundary conditions. The diffusion trajectory was subsequently used to generate simulated photon emissions of the diffusing particles from a simulated point spread function that is supplied with the PyBromo module. The PyBromo photon emission simulation procedure was adapted in order to achieve simulations of photon emissions according to the pulsed interleaved excitation (PIE) scheme. In order to achieve this, different photon emissions were simulated from the same particle diffusion trajectory to yield photon emissions for each desired FRET states, donor-only, acceptor-only, and as background counts. First, the donor-excited photon streams ($D_{ex}D_{em}$ and $D_{ex}A_{em}$) are simulated for each desired FRET state. The desired FRET value is defined together with the peak count rate that is desired for the simulated photon emissions. As detailed in the PyBromo documentation, the peak count rate is defined as the total count rate over the donor-excited photon streams. Therefore, the specific count rate in the donor and acceptor channels depend on the specified FRET efficiency. Next, the acceptor-excited photon emissions ($A_{ex}A_{em}$) are simulated from the same particle trajectory by setting the FRET efficiency to 1, which effectively simulated another acceptor photon stream. At this stage, static simulations of each desired FRET efficiency are generated by combining the donor-excited photon streams ($D_{ex}D_{em}$ and $D_{ex}A_{em}$) and the acceptor-excited photon stream ($A_{ex}A_{em}$). Since the $D_{ex}A_{em}$ and $A_{ex}A_{em}$ have the same detection channel, the photon streams are differentiated by assigning a unique value for these streams in the nanotime array. Additionally, the identity of each particle is saved. This is needed to be able to generate a continuous

sequence of visited FRET states in the subsequent simulation step.

In the following step, dynamics switching between FRET states is simulated based on the different donor- and acceptor-excited photon streams with different FRET efficiencies from the same particle diffusion trajectory. The transition between FRET states is simulated as a Markov sequence individually for the simulated photon emissions of each particle. The transition matrix of the Markov sequence defined the allowed state conductivities. The resulting sequence solely encodes the sequence of FRET states. The time that each simulated particle spends in a particular state is then drawn from an exponential distribution with the average set to the desired dwell time of the corresponding FRET state (for details on how the state dwell times can be converted to simulated state exchange rates see Supplementary Note 1). The photon emissions for each simulated particle with different FRET efficiencies are then combined, meaning that the simulated photon records are stitched together based on the simulated sequence of states, for the simulated (realized) dwell time of each state. This alternates the $D_{ex}D_{em}$ and $D_{ex}A_{em}$ emission patterns from the different desired FRET efficiencies and simulates instantaneous switching between discrete FRET states. Importantly, the FRET dynamics are simulated independently from blinking phenomena because those processes are considered here to be independent of each other.

In the final step, blinking dynamics were added *on top* of the dynamic simulations of FRET dynamics that were described in the previous paragraph. A Markov sequence was generated that describes the blinking sequence of state transitions for each simulated particle. To simulate blinking, the transition from each state to any other state was allowed, because we assume that donor and acceptor dye blinking to occur independently. In the same way as described in the previous paragraph, blinking dynamics are simulated by alternating between the photon emissions of the dynamic FRET system (referred to as "FRET-active states"), the donor-only emissions (generated by simulating photon emissions of each particle with a FRET efficiency of 0), and the acceptor-only emissions (already generated above with the $A_{ex}A_{em}$ photon stream). The exact dwell times of these states is given by defining the average dwell times and drawing from an exponential distribution. This simulation approach was chosen to eliminate any potential variability caused by differences of the particle diffusion trajectory (all simulated photon emissions are obtained from the same diffusion trajectory), it allows adding different blinking dynamics to the same simulation of a dynamic FRET system, and is less computationally intensive because different photon emissions are dynamically combined rather than simulated again. Furthermore, no intensity-dependent photophysical effects of the simulated dye emissions were considered in the simulation of dye blinking dynamics.

Parameters for the presented simulations

The PIE smFRET simulations used in the publication were generated from a Pybromo particle simulation with a simulation time step of $0.5\ \mu s$ and a total simulation time of $500\ s$. A number of 15 particles were simulated with a diffusion coefficient of $10\ \mu m^2/s$ in a simulation box with a size of $6\mu m \times 6\mu m \times 8\mu m$. The numeral point spread function provided with Pybromo was used for simulating photon emissions. The resulting particle trajectory file generated photon emissions with a peak count rate of $350\ kHz$, an acceptor count rate of $350\ kHz$, and donor and acceptor channel background count rates of $1.5\ kHz$, respectively. Simulations with FRET states $E_{LF} = 0.3$ and $E_{HF} = 0.5$ were generated and combined into PIE files, as described in the previous section. A dynamic simulation with a mean dwell time of $t_{LF} = 2.5\ ms$ and $t_{HF} = 1\ ms$ was created (dwell time can be converted to an exchange rate with $k_i = (ti)^{-1}; k_{LF\rightarrow HF} = 400\ s^{-1}, k_{HF\rightarrow LF} = 1000 s^{-1}$, see Supplementary Note 1). Blinking dynamics of different timescales were added to the smFRET simulation by performing a second round of dynamic exchange simulations between the dynamic simulation file, the donor-only emission file, and the acceptor-only emission file. The time in which the dynamic FRET simulation was active was defined as the dwell time of the FRET-active state. Additionally, the dwell times of the donor- and acceptor-only states were varied as such that the FRET-active state was always the longest state in a given simulation. The exact simulation parameters are listed in Suppl. Table 1.

Description of the computational environment

Data processing and computations were performed using the Python programming language (version 3.12.3) in a conda virtual environment with Numpy 1.26.4 [53, 54], matplotlib 3.9.2 [55], Numba 0.59.1 [56] in Jupyter computational notebooks [57, 58]. Data simulations were performed with Pybromo 0.8.1 [52] and saved as photon-HDF5 using the phconvert module [47]. Data analysis was performed with FRETBursts 0.8.3 [48, 49] and burstH2MM 0.1.7 [40, 51].

Results

mpH^{2}MM resolves short-lived dye states in seemingly clean data

Fluorescence data from free diffusion, confocal single-molecule FRET (smFRET) recordings include different types of burst events. Ideally, all burst events originate from molecules labeled with emissive 'FRET-active' donor and acceptor dyes reporting on the

structural state of the molecule of interest. Oftentimes, burst events stem from molecules with only one type of dye due to an incomplete labeling reaction or due to photobleaching. A commonly used way to detect non-FRET-active molecules is alternating donor and acceptor excitation, e.g. PIE, and displaying the raw data in the so-called $E-S$ plot. In this 2D histogram, the distribution of burst-averaged FRET efficiency (E) and stoichiometry (S) parameters is displayed. While E is a measure for the donor-acceptor distance, S reports on the relative brightness of the donor and acceptor dyes. Assuming equal brightnesses of the donor and acceptor, a molecule labeled with a single donor and acceptor dye will display a stoichiometry of 0.5, whereas a donor- or acceptor-only carrying molecule will assume values for S equal to 1 and 0, respectively.

To illustrate the $E-S$ plot, we carried out PIE-smFRET measurements of a pM solution of a dynamic DNA hairpin molecule. The equilibrium between the open, low FRET, and closed, high FRET states can be modulated with the concentration of NaCl [46]. We performed a burst search and calculated the burstwise E and S parameters. No corrections were applied to any of the shown data. The burst-averaged $E-S$ histogram of unfiltered data displayed four populations: a donor-only population (with $E \approx 0$ and $S \approx 1$), an acceptor-only population (with $S \approx 0$ and broad distribution in E), and two FRET states (with $S \approx 0.5$, $E_1 \approx 0.15$ and $E_2 \approx 0.65$) (Fig. 1A). Next, we removed the alleged

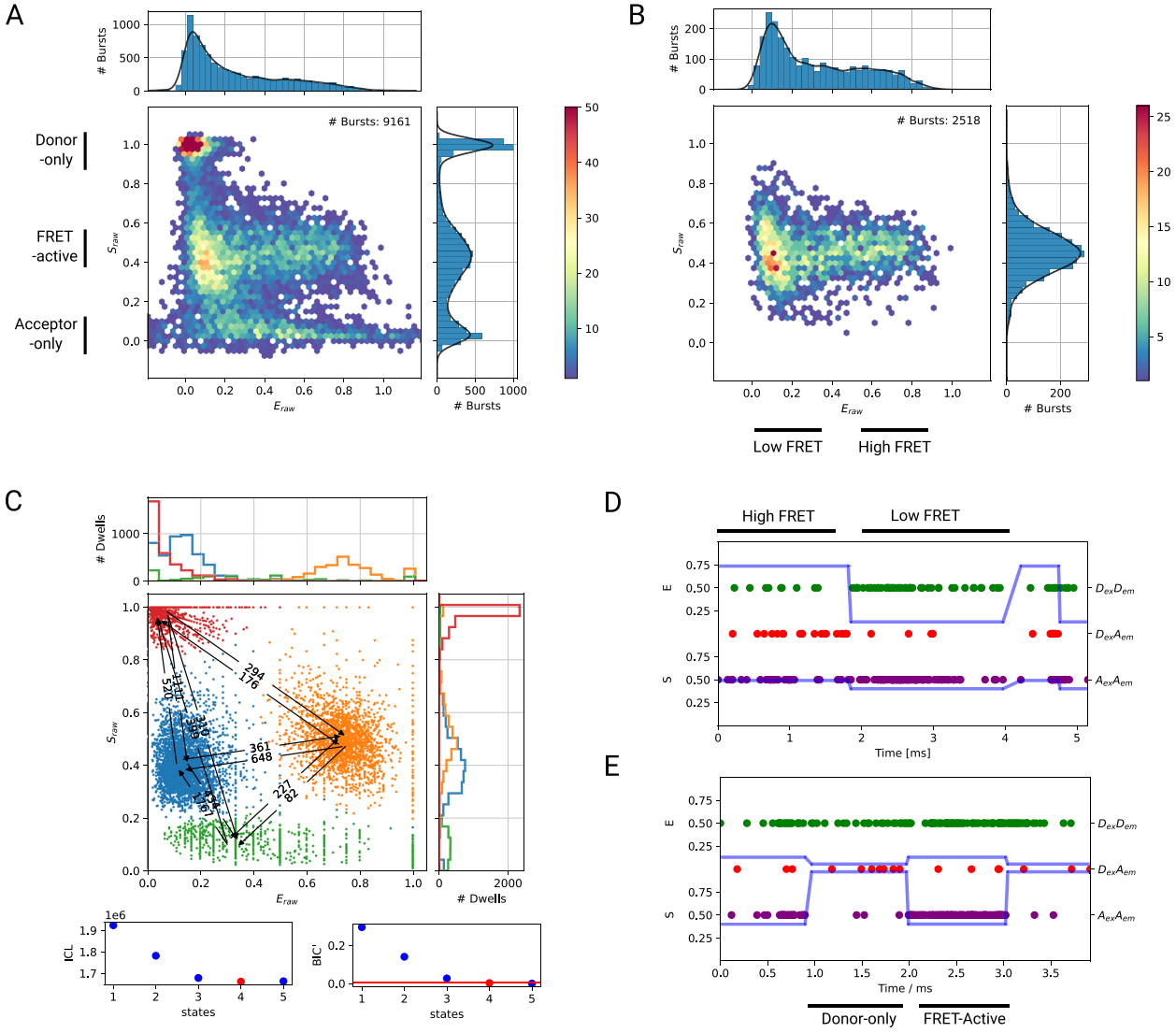

Fig. 1 smFRET data of a FRET-labeled dynamics DNA hairpin at 500 mM NaCl. **A** Burst-based $E-S$ plot of the data before and (**B**) after filtering for FRET-active bursts. **C** Dwell-based $E-S$ plot obtained after mpH^{2}MM analysis of the bursts shown in B. The ICL and BIC' plots indicate the optimal number of states. **D** and **E** Exemplary burst traces from the data shown in B. **D** shows an ideal event exclusively observed transitioning between FRET states, whereas (**E**) shows transitions between FRET-active and donor-only states

donor- and acceptor-only bursts by requiring per burst at least 60 FRET photons (in the $D_{ex}D_{em}$ or $D_{ex}A_{em}$ PIE channels) and 40 photons emitted by the acceptor upon acceptor excitation ($A_{ex}A_{em}$). The retained bursts display a single population in *S* with a value close to 0.5 and a broad distribution in *E*, indicating that the DNA hairpin was captured in several structural states (Fig. 1B).

We submitted the smFRET data from Fig. 1B to mpH^{2}MM analysis to determine the most likely number of states and their connectivity and to quantify the state exchange kinetics. The best-fitting number of visited states of the mpH^{2}MM fit was determined by consulting the ICL and BIC' plots, which take the model likelihood and number of parameters into account and allow choosing the optimal number of states present in the dataset. The mpH^{2}MM results indicated that four states optimally describe the data. We visualized the results as a dwell-based $E-S$ plot (Fig. 1C), which shows the *E* and *S* parameters of the duration that a burst was found in a particular state rather than the averaged *E* and *S* parameters of the whole burst (compared to Fig. 1A and B). We found two states with $E_1 \approx 0.15$ and $E_2 \approx 0.7$, both with an $S \approx 0.5$, which we interpreted as FRET-active states of the open and closed conformation of the DNA hairpin, respectively. The four-state mpH^{2}MM result reported state exchange rates of $350\ s^{-1}$ ($k_{LF\rightarrow HF}$) from low to high and $650\ s^{-1}$ from the high to low FRET-active states ($k_{HF\rightarrow LF}$). Two more states were resolved in the dwell-based $E-S$ plot with *S* values close to 1 and 0, which are clear signatures for donor-only and acceptor-only states, respectively. We interpreted these as states where the donor and acceptor dyes underwent transitions between FRET-active states and blinking states. The exchange rates obtained from the mpH^{2}MM result mostly returned rates of several hundred times per second for transitions to and from dye blinking states (Fig. 1C). We were interested in these short visits to blinking states in a burst duration from a seemingly blinking-free $E-S$ plot. We plotted the state trajectory obtained from the four-state mpH^{2}MM model (blue lines in Fig. 1D and E) with the individual PIE photon streams of exemplary bursts (green, red, and purple dots in Fig. 1D and E). In this way, we could closely examine the underlying raw photon data of bursts that were exclusively found in FRET-active states, by which we refer to bursts with an *S* close to 0.5 and thus exclusively informative on FRET states (Fig. 1D), as well as bursts containing temporary visits to donor- and/or acceptor-only states with corresponding fluctuations in *S* (Fig. 1E). Transitions between FRET-active states were evident in the state trajectories as a switch of the ratio between donor and acceptor photons upon donor excitation (see $D_{ex}D_{em}$ and $D_{ex}A_{em}$ photon streams in Fig. 1D). However, the photon streams of many bursts also contained changes in the number of photons of the acceptor upon acceptor excitation ($A_{ex}A_{em}$). In the example shown in Fig. 1E, this indicates that the acceptor dye temporarily stopped emitting fluorescence (marked as "donor-only" in Fig. 1E), which goes along with a corresponding drop in the calculated value for *E* to 0 and *S* to 1 during that off-time of the acceptor dye. During the off-time period, no changes in *E* can be detected, and therefore, no information on biomolecular dynamics can be obtained. The following section of the example burst trace in Fig. 1E is a low FRET state, followed again by a donor-only state. However, in this example burst, it is not clear whether the time in which mpH^{2}MM identified the DNA hairpin to be in the low FRET state is correct or if the observation time in which the molecule was in the low FRET state was interrupted by the blinking of the acceptor dye.

We explored other burst filtering approaches to remove bursts containing blinking and reanalyzed the same DNA hairpin dataset. We applied the ALEX-2CDE filter, an algorithm that allows differentiating between bursts that underwent fluctuations in *S* by calculating a filter value for each photon in a burst with a specified time window constant [38]. We submitted moderately and strictly ALEX-2CDE-filtered burst to mpH^{2}MM analysis. Again, many donor- and acceptor-only states were found by mpH^{2}MM (Figs. A1 and A2). As another approach to suppress to potentially decrease the proportion of bursts containing blinking dynamics, we performed DCBS on the DNA hairpin dataset in contrast to the all-photon burst search in the other analysis attempts. DCBS requires the presence of sufficient signal in both the donor and acceptor channels within a short time window to accept a burst event. DCBS can effectively remove bursts that exclusively display donor or acceptor signals due to photobleaching or incomplete labeling. Also, with DCBS-filtered data, donor- and acceptor-blinking states were still found by mpH^{2}MM analysis (Fig. A3). We compared the four-state mpH^{2}MM results of the photon-count thresholded bursts, the two ALEX-2CDE filters (moderate and strict filtering), and the DCBS-filtered bursts with regards to the proportion of bursts that were exclusively found in a FRET-active state ("F") or if a donor and/or acceptor blinking state was identified in the burst duration (Fig. A4A, "F-D" and "F-A" as combination of FRET-active and donor-only or acceptor-only states, respectively, or "F-D-A" as bursts with FRET-active, donor-only, and acceptor-only states). Compared to simple photon count thresholding, which had 22% of bursts exclusively in FRET-active states, ALEX-2CDE and DCBS increased the relative amount of bursts that exclusively contained FRET-active states, with strict ALEX-2CDE filtering being the most effective with about 40% of FRET-active bursts. However, the total number of bursts after moderate and strict ALEX-2CDE

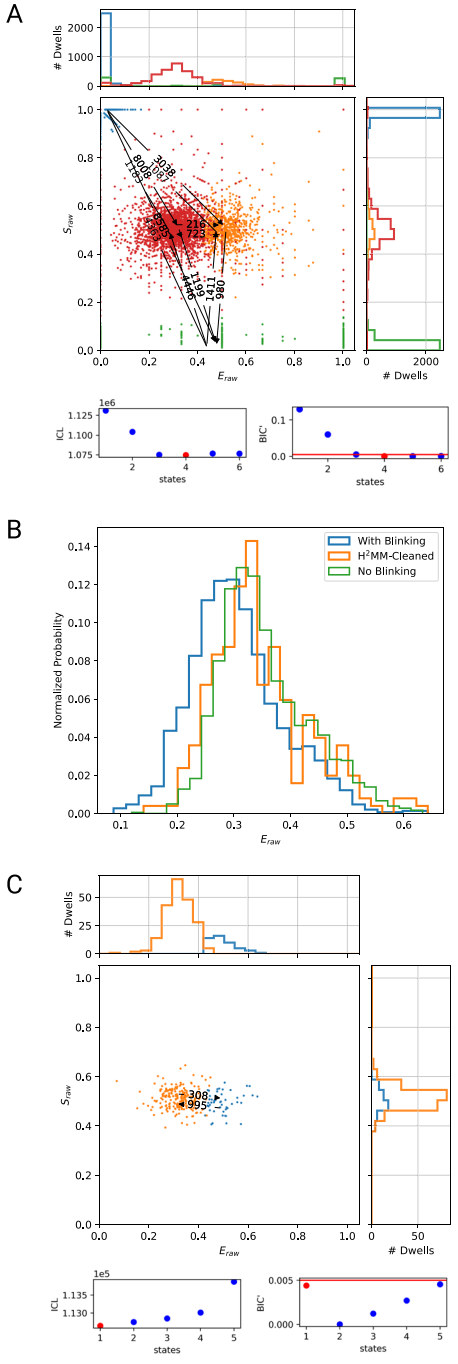

Fig. 2 Simulated smFRET data with blinking dynamics. **A** Dwell ES plot of the mpH^{2}MM result of a molecule dynamically exchanging between $E_{LF} = 0.3$ and $E_{HF} = 0.5$ with an exchange rate of $k_{LF\rightarrow HF} = 300\ s^{-1}$ and $k_{HF\rightarrow LF} = 1000\ s^{-1}$ and blinking dynamics with dwell times of the FRET-active state of $3\ ms$, the donor-only states of 0.5 ms and the acceptor-only states of $1\ ms$. **B** Burst FRET efficiency histograms of the simulated smFRET data with blinking dynamics (blue) after mpH^{2}MM-cleaning (orange), and the simulation without adding dye blinking dynamics (green). **C** Dwell-based $E-S$ plot of the mpH^{2}MM result of the mpH^{2}MM-cleaned dataset shown in A. The arrows in A and C indicate the state exchange rates in s^{-1}

filtering and DCBS was reduced compared to APBS by about 27%, 69%, and 33%, respectively. As a result, strict ALEX-2CDE filtering retained about 310 bursts that were exclusively identified in a FRET-active state. In comparison, photon-count thresholded data contained a total number of about 550 bursts exclusively in a FRET-active state (Fig. A4A).

Taken together, a detailed analysis of our experimental smFRET burst data from a dynamic DNA hairpin with mpH^{2}MM indicated the presence of short-lived, FRET-independent fluctuations of the donor and acceptor brightnesses. Filtering the data with state-of-the-art methods did not allow us to remove these erroneous bursts. We wondered if these fluctuations potentially interfere with analysis methods that aim at quantifying FRET dynamics experienced by the studied biomolecule.

mpH^{2}MM-guided removal of short-lived blinking states from filtered smFRET bursts

We assessed whether the presence of bursts with blinking dynamics would bias quantitative mpH^{2}MM analysis. Because in experimental samples the true kinetic and structural model is unknown, we turned to simulated smFRET data. We confirmed that mpH^{2}MM could correctly report simulated exchange rates from idealized simulations without blinking dynamics (Fig. A5). To explore the influence of dye blinking dynamics, we simulated particles that dynamically interconvert between two FRET states ($E_{LF} = 0.3, E_{HF} = 0.5$) with rates of $k_{LF\rightarrow HF} = 400\ s^{-1}$ and $k_{HF\rightarrow kLF} = 1.000\ s^{-1}$ (dwell times $t_{LF} = 2.5\ ms$ and $t_{HF} = 1\ ms$). Next, we added dye blinking dynamics to the two-state simulation, which was simulated to occur independently of FRET dynamics. We simulated blinking on a timescale similar to the FRET dynamics with a mean (drawn from a Markov process) donor-only dwell time of $0.5\ ms$, mean acceptor-only dwell time of $1\ ms$, and a mean FRET-active dwell time of $3\ ms$, which is the average time in which donor and acceptor are emissive ($k_{FRET-active\rightarrow D-only} = k_{FRET-active\rightarrow A-only} = 166\ s^{-1}$, $k_{D-only\rightarrow FRET-active} = k_{D-only\rightarrow A-only} = 1000\ s^{-1}$, $k_{A-only\rightarrow FRET-active} = k_{A-only\rightarrow D-only} = 500\ s^{-1}$).

We analyzed the simulations with mpH^{2}MM. The ICL and BIC' plots correctly indicated four states as the best-fitting model for the simulated data (Fig. 2A). However, we found that the state exchange rate constants returned by mpH^{2}MM between FRET states in the presence of blinking were about one-third lower than what we simulated, with $k_{LF\rightarrow HF} = 216\ s^{-1}$ and $k_{HF\rightarrow LF} = 723\ s^{-1}$. Additionally, we found that the burst E and S histograms appeared to shift towards lower values in the simulation with blinking dynamics compared to the simulation without blinking (Figs. 2B and A6).

Since mpH^{2}MM returns the most likely transition pathway between states for each burst, we wondered whether blinking-induced biases could be mitigated by simply removing bursts that were ever found in blinking-related states. From the four-state mpH^{2}MM result, we created a selection mask that excluded burst events that were ever identified as having visited blinking states as indicated by changes to states with a non-0.5 stoichiometry. The selection mask retained bursts found in E_{LF}, E_{HF}, or both in E_{LF} and E_{HF}. We applied this approach to the simulated smFRET data with blinking dynamics, which removed about 80% of burst events (273 of 1495 bursts left). We first compared the distribution of bursts on the $E-S$ plot of the simulated data without and with blinking dynamics to the bursts filtered for FRET-active states (heron referred to as 'mpH^{2}MM-cleaned'). The burstwise E plot from mpH^{2}MM-cleaned bursts better agreed with the burstwise distribution of the simulation before adding dye blinking dynamics (Fig. 2B, orange and green graphs, respectively). We analyzed the remaining bursts after mpH^{2}MM cleaning by resubmitting them to mpH^{2}MM analysis. The mpH^{2}MM-cleaned data was best described by a two-state model, as indicated by the BIC' plot, whereas the ICL plot assumed its lowest value for a one-state model. We plotted the two-state model and found results close to simulated E states ($E_{LF} = 0.31$, $E_{HF} = 0.49$) and the simulated rates between the FRET-active states were returned ($k_{LF\rightarrow HF} = 303\ s^{-1}$, $k_{HF\rightarrow LF} = 995\ s^{-1}$; Fig. 2C). Additionally, we plotted the three- and four-state models of the mpH^{2}MM run with the cleaned dataset and found no states that would correspond to donor or acceptor blinking states (Fig. A7A and B).

Because we observed that mpH^{2}MM returned a too-slow exchange rate in the presence of dye blinking dynamics from a simulated dataset with known parameters, we more systematically assessed the influence of blinking on mpH^{2}MM analysis. We used the same two-state smFRET simulation as before ($E_{LF} = 0.3$, $E_{HF} = 0.5$, $k_{LF\rightarrow HF} = 400\ s^{-1}$,$k_{HF\rightarrow kLF} = 1.000\ s^{-1}$). We added different degrees of blinking dynamics by varying the dwell times of the FRET-active state, which is the average time in which both donor and acceptor dyes are emissive and the donor-only and acceptor-only dwell times. As before, we analyzed the simulations with mpH^{2}MM, which returned a four-state model with two FRET-active, donor-only, and acceptor-only states (Suppl. Table 1). We plotted the obtained exchange rates between FRET states as a function of one of the simulated parameters, the FRET-active dwell time, i.e. the mean time molecules dwell in any FRET-active state after or before converting from or to either D- or A-only states. We found that the FRET state exchange rates reported by mpH^{2}MM were slower than the simulated rates with FRET-active dwell times shorter than $5\ ms$ (the average burst duration in the simulations was about $2\ ms$). Both the mpH^{2}MM-recovered $k_{LF\rightarrow HF}$ and $k_{HF\rightarrow LF}$ proportionally decreased to rates close to zero with the shortest FRET-active dwell time (Fig. 3A).

We applied our mpH^{2}MM-cleaning approach to the collection of simulated datasets with systematically varied blinking dynamics. We first noticed that the number of bursts that were retained after selecting bursts that were exclusively in FRET-active states was decreasing with more severe blinking dynamics. With FRET-active dwell times shorter than $1\ ms$, almost no bursts were left after mpH^{2}MM-cleaning. Those simulations were excluded from subsequent analysis (Fig. 3C). We reanalyzed the mpH^{2}MM-cleaned datasets. The ICL and BIC' plots mostly indicated a two-state model as optimum. The E and S parameters for the two FRET states were close to the simulated values for all simulations (Suppl. Table 1). We plotted the obtained exchange rates against the simulated FRET-active dwell time. We found that the values obtained after mpH^{2}MM-cleaning matched the simulated values more closely over a larger range of FRET-active dwell times (Fig. 3B, see horizontal orange and blue as simulated exchange rates).

mpH^{2}MM-cleaning of DNA hairpin smFRET data

We applied our proposed mpH^{2}MM-based filtering approach to the experimental smFRET data of a dynamic DNA hairpin (Fig. 1B and C). As demonstrated in the previous section, we used the four-state mpH^{2}MM model to remove those bursts from the dataset that were ever found to have visited a dye blinking state and effectively only retained bursts that were exclusively observed with emissive donor and acceptor dyes. The mpH^{2}MM-cleaning removed about 80% of the original burst events (553 of 2518 bursts left). As we observed with the simulated data, the burstwise histogram shifted towards higher values after mpH^{2}MM-cleaning. Furthermore, the population of low and high FRET bursts appeared equally populated, whereas more low FRET bursts were evident in the plot before mpH^{2}MM cleaning (Fig. 4A). We submitted the mpH^{2}MM-cleaned dataset to another round of mpH^{2}MM analysis. The ICL and BIC' plots indicated an optimal number of two E states of approximately 0.1 and 0.8 and stoichiometry close to 0.5, indicating that both states correspond to FRET-active states. No states were found that corresponded to dye blinking states. The exchange rates obtained from mpH^{2}MM analysis of the cleaned dataset were $k_{LF\rightarrow HF} = 470\ s^{-1}$ and $k_{HF\rightarrow LF} = 488\ s^{-1}$ (compared to $361\ s^{-1}$ and $648\ s^{-1}$, respectively, before mpH^{2}MM-cleaning) (Fig. 4B). To demonstrate the behavior of mpH^{2}MM-cleaning with other experimental dataset, we applied the approach to the DNA hairpin with a concentration

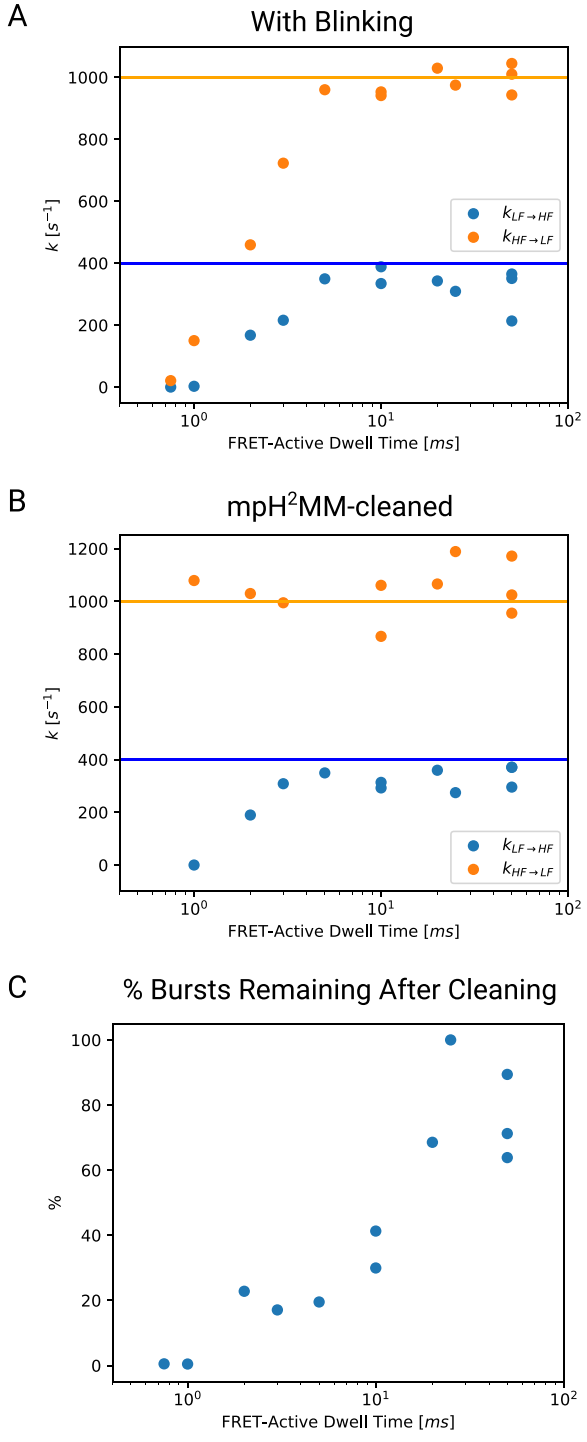

Fig. 3 Simulated smFRET data shows the influence of increased dye blinking and the ability of mpH^{2}MM-cleaning to reduce blinking-induced biases. **A** and **B** show the recovered exchange rate between E_{LF} and E_{HF} as a function of the dwell time of the FRET-active state before and after mpH^{2}MM-cleaning, respectively. The blue and orange lines indicate the simulated exchange rates between FRET states. **C** The remaining percentage of bursts after applying mpH^{2}MM cleaning to the data shown in A as a function of the FRET-active dwell time

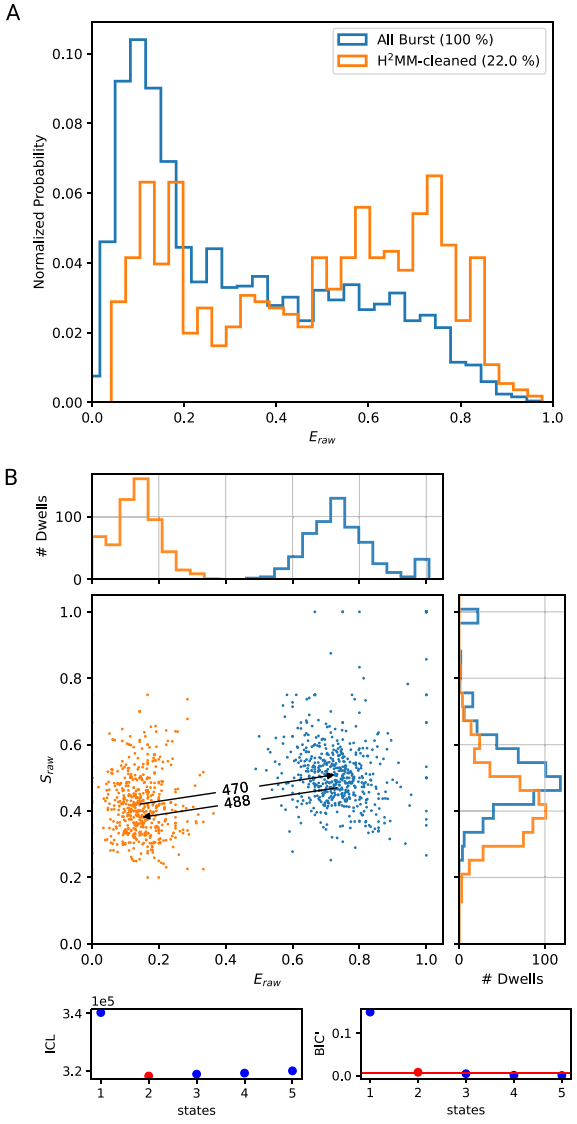

Fig. 4 Application of the mpH^{2}MM-cleaning approach to experimental data of a dynamic DNA hairpin with 500 mM NaCl. **A** Burstwise FRET efficiency plot of the dynamic DNA hairpin data before (blue) and after (orange) applying mpH^{2}MM-cleaning. **B** Dwell ES plot of the mpH^{2}MM results from the mpH^{2}MM-cleaned dataset. The arrows display the obtained transition rates between states. The ICL and BIC' plots below indicate the optimal number of states explaining the data

of NaCl of 300 mM which causes the DNA hairpin to occupy the high FRET states less due to less shielding of the backbone charges of molecule [46] (see Fig. A9). We also applied the approach to a mixture mixture of FRET-labeled DNA molecules to showcase how mpH^{2}MM-cleaning works with a static mixture of molecules (see Fig. A10). Also with the additional datasets, mpH^{2}MM identified blinking states that led to removing 82% and 67% of burst, for the DNA hairpin with 300 mM of NaCl and the mixture of static DNA molecules, respectively. For the DNA hairpin with 300 mM NaCl compared to the data with 500 mM NaCl, the exchange rates

between the high and low FRET states increased from about $500\ s^{-1}$ to about $1000\ s^{-1}$, whereas the rate from the low to the high FRET state decreased from about $500\ s^{-1}$ to about $250\ s^{-1}$. These changes of the exchange rates explain the observation that the low FRET state appears more populated with $300\ mM$ NaCl compared to $500\ mM$ (see Figs. 4 and A9).

Discussion

In this study, we systematically assessed the influence of dye blinking dynamics on quantitative analysis of smFRET burst data. We demonstrated that burst smFRET data contain short-lived dye-related artifacts even after additional processing with filtering methods such as ALEX-2CDE [38] or DCBS [50]. Using simulations, we demonstrated that blinking dynamics distort burst-averaged $E-S$ histograms and systematically cause mpH^{2}MM to underestimate the exchange rates between FRET states depending on the severity of dye blinking (Figs. 2A and 3A). We then proposed an mpH^{2}MM-guided approach to remove bursts that contain dye blinking, which considerably increased smFRET data quality, albeit at cost of a proportional loss of bursts (Fig. 3C).

We showed with simulated data that blinking dynamics systematically affect the FRET state exchange rates returned by mpH^{2}MM, even if blinking states are correctly accounted for in the model. In the presence of dye blinking on a timescale similar to the FRET dynamics, the exchange rates between FRET states reported by mpH^{2}MM were too slow (Fig. 3A). We also observed a shift of the burst-averaged E and S histograms, which results in obtaining too low values for these parameters (Figs. 2C and A6). Such effects have been described previously and depend on the occupancy of the fluorescent dyes in non-emissive triplet states, which vary depending on buffer composition, excitation intensity, and dye pair [33, 59, 60]. This again demonstrates that treating dye blinking is not only critical for the analysis of dynamics but also important when deriving distances from E histograms. Interestingly, we found here with our simulations that included blinking dynamics that the average values for E obtained from regular mpH^{2}MM analyses are unaffected by the blinking dynamics (Fig. A8). This demonstrates the effectiveness of photon-by-photon analysis over burst histogram-based analysis approaches where the presence of blinking dynamics did introduce a considerable shift of the histogram (see Figs. 2B and A6).

We proposed an mpH^{2}MM-guided burst cleaning approach that works by retaining only those bursts that were never found to visit a blinking state in their burst duration. This is possible because mpH^{2}MM obtains the state trajectory of each burst, which is then used to remove bursts that visited a donor- or acceptor-blinking state. We characterized the effects of removing blinking-affected bursts with simulated data. We found that the number of bursts that were removed depended on the severity of blinking dynamics (Fig. 3C). The bias of exchange rates between FRET states was mitigated by mpH^{2}MM-guided removal of blinking-affected bursts (Fig. 3B). Because mpH^{2}MM works on the level of photon-by-photon traces of individual burst events, it can detect blinking states much shorter than burst duration. The observation that mpH^{2}MM returns too slow FRET state exchange rates in the presence of severe blinking dynamics is likely attributed to the fact that fast blinking prematurely terminates FRET-active states. With fast blinking dynamics, the probability of observing a molecule transitioning from a FRET to a blinking state is higher than transitioning to another FRET state (see Supplementary Note 2). The mpH^{2}MM-guided cleaning approach may be further improved by considering the state trajectory that is returned by mpH^{2}MM analysis. Instead of discarding an entire burst that was ever found in a blinking state, more burst data can possibly be retained by only removing those parts of a burst that were pre- or succeeded by a blinking state. In future developments of the method, the mpH^{2}MM-cleaning approach could thus take the state trajectory into account to retain more data.

From our experimental smFRET data of a dynamic DNA hairpin labeled with state-of-the-art fluorescent dyes, Alexa Fluor 488 and ATTO 643, about 80% of bursts had to be removed because they contained short-lived blinking states (Figs. 1E and 4A). We also attempted to remove blinking-affected burst events using different filtering techniques, such as ALEX-2CDE [38] or DCBS [50] (Figs. A1 and A2). While we found that these methods increase the relative number of bursts that exclusively contain FRET dynamics (Fig. A4A), there is an overproportional loss of burst events and, thus, a loss of data that contained FRET-relevant information. With the presented DNA hairpin data, the photon-thresholded bursts contained 22% of bursts exclusively identified in FRET states (553 of 2518 bursts). In comparison, strict filtering with the ALEX-2CDE approach increased the proportion to over 40% (Fig. A4A). Strict ALEX-2CDE only retained a total of about 300 bursts solely in FRET-active states, while the mpH^{2}MM data analysis without additional ALEX-2CDE filtering identified 550 FRET-active bursts. Although the proportion of FRET-relevant bursts was clearly improved, a significant number of bursts was lost that contained information on FRET-relevant transitions. The mpH^{2}MM result also allowed us to visualize the position of bursts on the $E-S$ plot depending on how much time they were found to spend in a blinking state as a fraction of the respective burst duration (Fig. A4B). Deviations of a burst in the S histogram indicate that

blinking is likely contained in the burst photon traces. However, the gradual distribution of the time a burst was found in blinking states shows the difficulty of getting rid of blinking dynamics on the level of the $E-S$ plot, for example, by thresholding data in S. We explored this phenomenon further with the simulated dataset from Fig. 2 with known blinking dynamics (FRET-active dwell time of 3 ms, donor-only dwell time of 0.5 ms and an acceptor-only dwell time of 1 ms). Given this blinking regime, we found that the proportion of bursts with only FRET-relevant information (F) is much reduced. Also, under these conditions, the effectiveness of ALEX-2CDE and DCBS with regard to increasing the content of F bursts appears impeded (see Fig. A11). However, with a less severe blinking regime of the same simulated FRET system (FRET-active dwell time of 15 ms, donor-only and acceptor-only dwell times of 5 ms), ALEX-2CDE- and DCBS-based filtering behave similarly to what we have observed with actual experimental data (see Fig. A12). This shows the complexity of how the timescale of the blinking dynamics interacts with the burst duration. Given sufficiently fast blinking dynamics (as shown in Figs. 2 and A11), the ability of any method to retain bursts with only FRET-relevant information is simply limited by the fact that all bursts contain blinking states (see Supplementary Note 2). This is also demonstrated by the fact that the loss of bursts events after mpH2MM-cleaning is correlated with the severity of blinking (see Fig. 3C).

Our results demonstrate the need to consider dye blinking in smFRET data analysis and to investigate if data is significantly affected by blinking. Typically, this is done by analyzing the data with fluorescence correlation methods (FCS) and fitting to a model that takes photophysics-induced fluctuations into account [61, 62]. However, it can be difficult to differentiate between FRET- and dye-associated fluctuations. This is comparably simple with mpH^{2}MM by taking the S of the identified states into account. Furthermore, we want to emphasize that approaches to reduce blinking dynamics are worth exploring to improve smFRET data quality and minimize the need for computationally correcting the data. The usage of oxygen-quenching systems, for example, has been shown to reduce blinking dynamics in smFRET data [31, 34]. However, if optimization efforts did not alleviate the impact of dye blinking in a particular experimental context, mpH^{2}MM-cleaning may be useful as a computational way to remove the influence of blinking dynamics. We thus consider mpH^{2}MM-cleaning as a valuable tool for removing blinking-affected bursts and as a computational way to improve the quality of burst smFRET data. Removing states from burst datasets, which can certainly be assigned as a donor or acceptor blinking state, simplifies the analysis of underlying data and allows using models that do not need to take photophysical phenomena, such as dye blinking, explicitly into account. Furthermore, the mpH^{2}MM-based removal of blinking states may be useful in combination with other quantitative analysis methods. Recent work by Terterov et al. (2024) [63] introduced a model-free approach that derives FRET efficiency correlation functions from photon-by-photon traces, independent of assumptions about discrete states. Such a model-free approach may be particularly useful when analyzing molecules that exhibit a distribution of conformations rather than discrete FRET states, such as intrinsically disordered proteins [64]. In contrast, mpH^{2}MM assumes a fixed number of discrete states, which requires careful model selection [40]. Future work could explore the combination of mpH^{2}MM-guided burst cleaning with, for example, model-free correlation approaches to better disentangle photophysical effects from true conformational dynamics in burst smFRET data.

Conclusion

We demonstrated here that short-lived dye blinking states persist in standard-practice filtered burst smFRET data, biasing both the $E-S$ plot distribution and quantitative analyses by, for example, mpH^{2}MM. We presented an mpH^{2}MM-based burst filtering approach that removes blinking-contaminated bursts, allowing us to accurately recover kinetic information from burst smFRET data. While our method reduces the number of bursts proportionally to the severity of blinking dynamics, mpH^{2}MM-cleaning retains high-quality data, allowing us to accurately determine dynamic transition rates. Our method complements experimental strategies for reducing the impact of dye blinking on smFRET data quality. It seamlessly integrates into existing mpH^{2}MM workflows, providing a straightforward computational solution to mitigate blinking-induced biases.

Supplementary Information

The online version contains supplementary material available at https://doi.org/10.1186/s44330-025-00039-2.

Supplementary Material 1.

Supplementary Material 2.

Acknowledgements

The authors would like to acknowledge Stijn Dilissen (Dynamic Bioimaging Lab, Hasselt University) for preparing and measuring the dynamic DNA hairpin presented in this work. We acknowledge the Advanced Optical Microscopy Centre at Hasselt University for support with the microscopy experiments.

Authors' contributions

TK and JH conceptualized the study and wrote the main text. TK carried out the simulations and analysis.

Funding

This work was funded by the Flemish Research Foundation (***Fonds Wetenschappelijk Onderzoek***, FWO) with grant numbers 11N4722N and G0B9922 and the UHasselt Special Research Fund (21INC20BOF and 20KP14BOF).

Data availability
The code used to analyze the presented experimental smFRET data, the code used to generate the smFRET simulations, and the code to perform mpH2MM-based cleaning of blinking events is provided on Zenodo (https://zenodo.org/records/14919597).

Declarations

Ethics approval and consent to participate
Not applicable.

Consent for publication
Not applicable.

Competing interests
The authors declare no competing interests.

Received: 25 February 2025 / Accepted: 30 June 2025
Published online: 07 August 2025

References

1. Lerner E, Cordes T, Ingargiola A, Alhadid Y, Chung S, Michalet X, et al. Toward dynamic structural biology: two decades of single-molecule Förster resonance energy transfer. Science. 2018;359(6373):eaan1133. https://doi.org/10.1126/science.aan1133.
2. Lerner E, Barth A, Hendrix J, Ambrose B, Birkedal V, Blanchard SC, et al. FRET-based dynamic structural biology: Challenges, perspectives and an appeal for open-science practices. eLife. 2021;10:e60416. https://doi.org/10.7554/eLife.60416.
3. Nettels D, Galvanetto N, Ivanović MT, Nüesch M, Yang T, Schuler B. Single-molecule FRET for probing nanoscale biomolecular dynamics. Nat Rev Phys. 2024;6(10):587–605. https://doi.org/10.1038/s42254-024-00748-7.
4. Haran G, Mazal H. How fast are the motions of tertiary-structure elements in proteins? J Chem Phys. 2020;153(13):130902. https://doi.org/10.1063/5.0024972.
5. Mazal H, Haran G. Single-molecule FRET methods to study the dynamics of proteins at work. Curr Opin Biomed Eng. 2019;12:8–17. https://doi.org/10.1016/j.cobme.2019.08.007.
6. Hamilton GL, Saikia N, Basak S, Welcome FS, Wu F, Kubiak J, et al. Fuzzy super-tertiary interactions within PSD-95 enable ligand binding. eLife. 2022;11. https://doi.org/10.7554/eLife.77242.
7. Mader SL, Lopez A, Lawatscheck J, Luo Q, Rutz DA, Gamiz-Hernandez AP, et al. Conformational dynamics modulate the catalytic activity of the molecular chaperone Hsp90. Nat Commun. 2020;11(1):1410. https://doi.org/10.1038/s41467-020-15050-0.
8. Aviram HY, Pirchi M, Mazal H, Barak Y, Riven I, Haran G. Direct observation of ultrafast large-scale dynamics of an enzyme under turnover conditions. Proc Natl Acad Sci U S A. 2018;115(13):3243–8. https://doi.org/10.1073/pnas.1720448115.
9. Heitkamp T, Börsch M. Fast ATP-dependent Subunit Rotation in reconstituted FoF1-ATP synthase trapped in Solution. Biophysics. 2021. https://doi.org/10.1101/2021.03.21.436299.
10. Maslov I, Volkov O, Khorn P, Orekhov P, Gusach A, Kuzmichev P, et al. Sub-millisecond conformational dynamics of the A2A adenosine receptor revealed by single-molecule FRET. Commun Biol. 2023;6(1):362. https://doi.org/10.1038/s42003-023-04727-z.
11. van den Noort M, Drougkas P, Paulino C, Poolman B. The substrate-binding domains of the osmoregulatory ABC importer OpuA transiently interact. eLife. 2024;12. https://doi.org/10.7554/elife.90996.3.
12. Sefer A, Kallis E, Eilert T, Röcker C, Kolesnikova O, Neuhaus D, et al. Structural dynamics of DNA strand break sensing by PARP-1 at a single-molecule level. Nat Commun. 2022;13(1):6569. https://doi.org/10.1038/s41467-022-34148-1.
13. Harris PD, Hamdan SM, Habuchi S. Relative Contributions of Base Stacking and Electrostatic Repulsion on DNA Nicks and Gaps. J Phys Chem B. 2020;124(47):10663–72. https://doi.org/10.1021/acs.jpcb.0c06941.
14. Lerner E, Ingargiola A, Weiss S. Characterizing highly dynamic conformational states: The transcription bubble in RNAP-promoter open complex as an example. J Chem Phys. 2018;148(12):123315. https://doi.org/10.1063/1.5004606.
15. Kim C, Lee OC, Kim JY, Sung W, Lee NK. Dynamic release of bending stress in short dsDNA by formation of a kink and forks. Angew Chem Int Ed Engl. 2015;54(31):8943–7. https://doi.org/10.1002/anie.201502055.
16. Wozniak AK, Schroder GF, Grubmuller H, Seidel CAM, Oesterhelt F. Single-molecule FRET measures bends and kinks in DNA. Proc Natl Acad Sci. 2008;105(47):18337–42. https://doi.org/10.1073/pnas.0800977105.
17. Hatzakis NS. Single molecule insights on conformational selection and induced fit mechanism. Biophys Chem. 2014;186:46–54. https://doi.org/10.1016/j.bpc.2013.11.003.
18. Okazaki KI, Takada S. Dynamic energy landscape view of coupled binding and protein conformational change: induced-fit versus population-shift mechanisms. Proc Natl Acad Sci U S A. 2008;105(32):11182–7. https://doi.org/10.1073/pnas.0802524105.
19. Ha T, Fei J, Schmid S, Lee NK, Gonzalez RL Jr, Paul S, et al. Fluorescence resonance energy transfer at the single-molecule level. Nat Rev Methods Prim. 2024;4(1). https://doi.org/10.1038/s43586-024-00298-3.
20. Förster T. Energy migration and fluorescence. 1946. J Biomed Opt. 2012;17(1):011002. https://doi.org/10.1117/1.JBO.17.1.011002.
21. Kim Y, Ho SO, Gassman NR, Korlann Y, Landorf EV, Collart FR, et al. Efficient Site-Specific Labeling of Proteins via Cysteines. Bioconjug Chem. 2008;19(3):786–91. https://doi.org/10.1021/bc7002499.
22. Zosel F, Holla A, Schuler B. Labeling of proteins for single-molecule fluorescence spectroscopy. Methods Mol Biol (Clifton, NJ). 2022;2376:207–33. https://doi.org/10.1007/978-1-0716-1716-8_12.
23. Modesti M. Fluorescent labeling of proteins. In: Methods in Molecular Biology. Methods in molecular biology (Clifton, N.J.). New York: Springer New York; 2018. pp. 115–134. https://doi.org/10.1007/978-1-4939-7271-5_6.
24. Deniz AA, Dahan M, Grunwell JR, Ha T, Faulhaber AE, Chemla DS, et al. Single-pair fluorescence resonance energy transfer on freely diffusing molecules: Observation of Förster distance dependence and subpopulations. Proc Natl Acad Sci U S A. 1999;96(7):3670–5. https://doi.org/10.1073/pnas.96.7.3670.
25. Müller BK, Zaychikov E, Bräuchle C, Lamb DC. Pulsed Interleaved Excitation. Biophys J. 2005;89(5):3508–22. https://doi.org/10.1529/biophysj.105.064766.
26. Torella JP, Holden SJ, Santoso Y, Hohlbein J, Kapanidis AN. Identifying Molecular Dynamics in Single-Molecule FRET Experiments with Burst Variance Analysis. Biophys J. 2011;100(6):1568–77. https://doi.org/10.1016/j.bpj.2011.01.066.
27. Kalinin S, Felekyan S, Valeri A, Seidel CAM. Characterizing multiple molecular states in single-molecule multiparameter fluorescence detection by probability distribution analysis. J Phys Chem B. 2008;112(28):8361–74. https://doi.org/10.1021/jp711942q.
28. Santoso Y, Torella JP, Kapanidis AN. Characterizing Single-Molecule FRET Dynamics with Probability Distribution Analysis. ChemPhysChem. 2010;11(10):2209–19. https://doi.org/10.1002/cphc.201000129.
29. Felekyan S, Kalinin S, Valeri A, Seidel CAM. Filtered FCS and species cross correlation function. In: Multiphoton Microscopy in the Biomedical Sciences IX, vol. 7183. SPIE; 2009. pp. 93–106. https://doi.org/10.1117/12.814876.
30. Felekyan S, Sanabria H, Kalinin S, Kühnemuth R, Seidel CAM. Analyzing Förster resonance energy transfer with fluctuation algorithms. In: Methods in Enzymology. Methods in enzymology. Elsevier; 2013. pp. 39–85. https://doi.org/10.1016/b978-0-12-405539-1.00002-6.
31. Stennett EMS, Ciuba MA, Levitus M. Photophysical processes in single molecule organic fluorescent probes. Chem Soc Rev. 2014;43(4):1057–75. https://doi.org/10.1039/c3cs60211g.
32. Sabanayagam CR, Eid JS, Meller A. Long time scale blinking kinetics of cyanine fluorophores conjugated to DNA and its effect on Förster resonance energy transfer. J Chem Phys. 2005;123(22):224708. https://doi.org/10.1063/1.2136157.
33. Vandenberk N, Barth A, Borrenberghs D, Hofkens J, Hendrix J. Evaluation of blue and far-red dye pairs in single-molecule Förster resonance energy transfer experiments. J Phys Chem B. 2018;122(15):4249–66. https://doi.org/10.1021/acs.jpcb.8b00108.
34. Dey SK, Pettersson JR, Topacio AZ, Das SR, Peteanu LA. Eliminating spurious zero-efficiency FRET states in diffusion-based single-molecule confocal microscopy. J Phys Chem Lett. 2018;9(9):2259–65. https://doi.org/10.1021/acs.jpclett.8b00362.
35. Ha T, Tinnefeld P. Photophysics of fluorescent probes for single-molecule biophysics and super-resolution imaging. Annu Rev Phys Chem. 2012;63(1):595–617. https://doi.org/10.1146/annurev-physchem-032210-103340.
36. Lee NK, Kapanidis AN, Wang Y, Michalet X, Mukhopadhyay J, Ebright RH, et al. Accurate FRET measurements within single diffusing biomolecules using alternating-laser excitation. Biophys J. 2005;88(4):2939–53. https://doi.org/10.1529/biophysj.104.054114.
37. Hendrix J, Lamb DC. Pulsed Interleaved Excitation. In: Methods in Enzymology, vol. 518. Elsevier; 2013. pp. 205–243. https://linkinghub.elsevier.com/retrieve/pii/B9780123884220000091.

38. Tomov TE, Tsukanov R, Masoud R, Liber M, Plavner N, Nir E. Disentangling Subpopulations in Single-Molecule FRET and ALEX Experiments with Photon Distribution Analysis. Biophys J. 2012;102(5):1163–73. https://doi.org/10.1016/j.bpj.2011.11.4025.
39. Pirchi M, Tsukanov R, Khamis R, Tomov TE, Berger Y, Khara DC, et al. Photon-by-Photon Hidden Markov Model Analysis for Microsecond Single-Molecule FRET Kinetics. J Phys Chem B. 2016;120(51):13065–75. https://doi.org/10.1021/acs.jpcb.6b10726.
40. Harris PD, Narducci A, Gebhardt C, Cordes T, Weiss S, Lerner E. Multi-parameter photon-by-photon hidden Markov modeling. Nat Commun. 2022;13(1):1000. https://doi.org/10.1038/s41467-022-28632-x.
41. Joron K, Zamel J, Dvir S, Kalisman N, Lerner E. The structural basis for the self-inhibition of DNA binding by apo-σ^{70}. bioRxiv. 2022. https://doi.org/10.1101/2022.10.14.512049.
42. Han Z, Panhans S, Brameyer S, Bilgen E, Ram M, Herr A, et al. Dissecting mechanisms of ligand binding and conformational changes in the glutamine-binding protein. bioRxiv. 2023. https://doi.org/10.1101/2023.08.02.551720.
43. Gopich IV, Szabo A. Decoding the pattern of photon colors in single-molecule FRET. J Phys Chem B. 2009;113(31):10965–73. https://doi.org/10.1021/jp903671p.
44. Chung HS, Gopich IV. Fast single-molecule FRET spectroscopy: theory and experiment. Phys Chem Chem Phys. 2014;16(35):18644–57. https://doi.org/10.1039/c4cp02489c.
45. Harris PD, Lerner E. Identification and quantification of within-burst dynamics in singly labeled single-molecule fluorescence lifetime experiments. Biophys Rep. 2022;2(3). https://doi.org/10.1016/j.bpr.2022.100071.
46. Tsukanov R, Tomov TE, Berger Y, Liber M, Nir E. Conformational Dynamics of DNA Hairpins at Millisecond Resolution Obtained from Analysis of Single-Molecule FRET Histograms. J Phys Chem B. 2013;117(50):16105–9. https://doi.org/10.1021/jp411280n.
47. phconvert 0.9.1. https://photon-hdf5.github.io/phconvert/. Accessed 19 Nov 2024.
48. OpenSMFS. FRETBursts: 0.8.3. https://opensmfs.github.io/FRETBursts/. Accessed 2 Aug 2024.
49. Ingargiola A, Lerner E, Chung S, Weiss S, Michalet X. FRETBursts: An Open Source Toolkit for Analysis of Freely-Diffusing Single-Molecule FRET. PLoS ONE. 2016;11(8):e0160716. https://doi.org/10.1371/journal.pone.0160716.
50. Nir E, Michalet X, Hamadani KM, Laurence TA, Neuhauser D, Kovchegov Y, et al. Shot-noise limited single-molecule FRET histograms: comparison between theory and experiments. J Phys Chem B. 2006;110(44):22103–24. https://doi.org/10.1021/jp063483n.
51. Harris PD. bursth2mm 0.1.7. https://github.com/harripd/burstH2MM. Accessed 19 Nov 2024.
52. Ingargiola A. OpenSMFS/PyBroMo: Version 0.8.1. https://zenodo.org/records/3256149. Accessed 2 Aug 2024.
53. NumPy 1.26.4. Accessed 19 Nov 2024.
54. Harris CR, Millman KJ, van der Walt SJ, Gommers R, Virtanen P, Cournapeau D, et al. Array programming with NumPy. Nature. 2020;585(7825):357–62. https://doi.org/10.1038/s41586-020-2649-2.
55. Hunter JD. Matplotlib: a 2D graphics environment. Comput Sci Eng. 2007;9(3):90–5. https://doi.org/10.1109/mcse.2007.55.
56. Lam SK, Pitrou A, Seibert S. Numba. In: Proceedings of the Second Workshop on the LLVM Compiler Infrastructure in HPC. New York: ACM; 2015. https://doi.org/10.1145/2833157.2833162.
57. Jupyter 5.7.2. https://jupyter.org/.
58. Kluyver T, Ragan-Kelley B, Pérez F, Granger B, Bussonnier M, Frederic J, et al. Jupyter Notebooks - a publishing format for reproducible computational workflows. International Conference on Electronic Publishing. 2016. pp. 87–90. https://doi.org/10.3233/978-1-61499-649-1-87.
59. Vogelsang J, Doose S, Sauer M, Tinnefeld P. Improving single-molecule FRET measurements by confining molecules in nanopipettes. In: Popp J, von Bally G, editors. Biophotonics 2007: Optics in Life Science. SPIE; 2007. https://doi.org/10.1117/12.727842.
60. Pati AK, Kilic Z, Martin MI, Terry DS, Borgia A, Bar S, et al. Recovering true FRET efficiencies from smFRET investigations requires triplet state mitigation. Nat Methods. 2024;21(7):1222–30. https://doi.org/10.1038/s41592-024-02293-8.
61. Sakhapov D, Gregor I, Karedla N, Enderlein J. Measuring photophysical transition rates with fluorescence correlation spectroscopy and antibunching. J Phys Chem Lett. 2022;13(21):4823–30. https://doi.org/10.1021/acs.jpclett.2c00896.
62. Schönle A, Von Middendorff C, Ringemann C, Hell SW, Eggeling C. Monitoring triplet state dynamics with fluorescence correlation spectroscopy: bias and correction: MONITORING DARK STATE DYNAMICS WITH FCS. Microsc Res Tech. 2014;77(7):528–36. https://doi.org/10.1002/jemt.22368.
63. Terterov I, Nettels D, Lastiza-Male T, Bartels K, Loew C, Vancraenenbroeck R, et al. Model-free photon analysis of diffusion-based single-molecule FRET experiments. bioRxiv. 2024. https://doi.org/10.1101/2024.10.31.621265.
64. Schuler B, Soranno A, Hofmann H, Nettels D. Single-molecule FRET spectroscopy and the polymer physics of unfolded and intrinsically disordered proteins. Annu Rev Biophys. 2016;45:207–31. https://doi.org/10.1146/annurev-biophys-062215-010915.

Publisher's Note